Optimal Traffic Signal Control of Isolated Oversaturated Intersections Using Predicted Demand

Reza Mohajerpoor, Chen Cai, and Mohsen Ramezani

***Abstract*— This paper tackles the optimal traffic signal control of isolated oversaturated intersections. An analytical signal control algorithm is proposed to find the global optimal signal timings with dynamic cycle lengths and phase splits to minimize the vehicle delay throughout the oversaturation period at a generic multi-phase junction. The traffic dynamics are modelled based on the kinematic wave theory and the predicted traffic flows. Moreover, spillback avoidance is incorporated during the queue formation oversaturated regime by adopting a mixed delay and probability of spillback objective function. Microsimulation experiments demonstrate the optimality, practicality, and robustness to system uncertainties of the proposed signal control method. The results pinpoint over 63%, 55%, and 40% reduction in total vehicle delay by implementing the proposed signal control respectively compared to an optimal fixed-time, actuated, and capacity-aware max pressure signal control methods.**

***Index Terms*— Shockwave theory, fundamental diagram, convex optimization, queue spillover, urban networks.**

I. Introduction

A. Background and Motivation

CONTROL of signalized intersections can be categorized into isolated [1], [2], arterial [3], [4], and network levels [5], [6], [7]. The traffic signal control problem remains a major challenge at all of these levels during the oversaturated traffic conditions [4], [8]. The problem is exacerbated due to the low storage capacity at the links that results in the queue spillback events, which can spread and result in network gridlock. It has been shown in studies such as [9], [10], and [11] that the performance of commercial software packages often gets deteriorated in oversaturated traffic conditions. Therefore, it is crucial to efficiently address traffic signal control of oversaturated intersections in urban networks.

Recent methodological advancements in network Macroscopic Fundamental Diagram (MFD) offer an opportunity to devise perimeter flow control strategies. Those traffic congestion control schemes are network-level methods that are implementable by coordinated and adaptive control of a group of traffic signals located on the boundary of the network subregions [6], [12], [13]. Albeit their success in controlling the congestion inside the regions, when implementing perimeter control strategies, the intersections on the regions' boundary can get locally *oversaturated* congested as a bi-product [13], [14]. Therefore, it is imperative to consider and handle the accumulated residual queues at those intersections during the gating activation in the shortest possible time [14].

Traffic oversaturation can be categorized into queue formation (QF) and queue discharging (QD) regimes. An intersection is oversaturated when the residual queues of one or multiple major movements cannot be fully discharged within the green time allocated to those movements. The QF period refers to the beginning of the oversaturation period where the residual queues grow over time. The QD period follows the QF period where the demand has declined and the accumulated residual queues can be discharged. Moreover, a major movement of a phase is the critical movement of the phase with highest demand over saturation flow ratio.

Provided the overview on the literature of traffic signal control in Section I-B, the control of oversaturated intersections brings more challenges to traffic flow modelling, cycle-by-cycle residual queue variations, link capacity limitations, and uncertainties in the demand. In particular, most of the studies have overlooked the QF oversaturated traffic regimes, where demand is higher than the intersection's capacity. This paper proposes a Future demand based Adaptive Signal Control (FASC) algorithm, as a proactive and pragmatic approach to overcome this problem for a single intersection. The problem is challenging, as the impact of residual queues accumulated or discharged in each cycle passes on to the next cycles. The proposed control and optimization algorithm can be extended to multiple intersections along a major corridor, by accounting for the offsets as additional control parameters, a subject for future studies.

The FASC control strategy is proactive in instantly finding the *optimal cycle times and phase splits* for the whole duration of the queue formation and discharging traffic regimes at the start of each period. The proposed algorithm combines predictive and model-based strategies to achieve proactiveness and optimality. Numerical experiments demonstrate that FASC algorithm is computationally efficient and can be implemented with limited input measurement data and even interrupted online readings of traffic volumes. The low computational complexity of the algorithm is due to avoiding intractable microsimulation runs and iterative optimization

Manuscript received 27 April 2022; revised 9 September 2022; accepted 22 September 2022. The Associate Editor for this article was C. F. Mecklenbräuker. *(Corresponding author: Mohsen Ramezani.)*

Reza Mohajerpoor was with the School of Civil Engineering, The University of Sydney, Camperdown, NSW 2006, Australia, and also with the Data61, CSIRO, Eveleigh, NSW 2015, Australia.

Chen Cai is with the Data61, CSIRO, Eveleigh, NSW 2015, Australia.

Mohsen Ramezani is with the School of Civil Engineering, The University of Sydney, Camperdown, NSW 2006, Australia (e-mail: mohsen.ramezani@sydney.edu.au).

Digital Object Identifier 10.1109/TITS.2022.3209606

operations. Therefore, the proposed signal control scheme pertains strong practical perspectives that make it viable for field implementations.

B. Related Works

A large body of the literature tackles undersaturated intersections where the demand at the intersection is below its capacity (see e.g. [15], [16]). Traditional online and offline signal control packages employ traffic responsive heuristic optimization algorithms that make them workable for undersaturated traffic regimes [17], [18], [19], [20], [21]. Actuated-adaptive control schemes such as SCOOT [20] and SCATS [21] are non-model-based, which make them appropriate for large-scale networks. On the other hand, strategies such as PRODYN, TRANSYT [19], OPAC [18], and SYNCHRO [17] are model-based and employ dynamic programming or genetic algorithms in optimizing the cycle time and phase splits that often implies immense computational costs and obliges them to be applied to isolated or a few intersections. To speed up the optimization process of the signal control strategies, [22] proposed an approximate dynamic programming technique empowered by reinforcement learning algorithms.

A group of studies on intersection traffic signal control has concentrated on the distributed control of numerous connected intersections in a network using queuing/LWR theories or cell transmission models (CTM) (see e.g. [23], [24], [25]). Among these contributions, the max-pressure approach [26], [27], employs the queuing theory and attempts to maximize the throughput, while taking the pressure from the downstream queues into account. They showed the network stability assuming unlimited link storage capacities. Gregoire *et al.* [28] proposed a normalization method to account for finite link capacity (capacity-aware max-pressure). Further, Li and Jabari [29] proposed a decentralized max-pressure-based method that captures the spatial distribution of vehicles along the links and potential spillback conditions, which outperforms the standard and the capacity-aware max-pressure methods specifically in case of higher demands. The max-pressure method is employed in [30] to stabilize the queues in signalized arterials. The majority of the CTM-based distributed signal control frameworks either (i) replace nonlinear fundamental flow-density relationships by linear inequalities to lessen the computational complexity, or (ii) apply nonlinear fundamental traffic relationships. The former approach results in the flow holding back phenomena due to inaccurate traffic flow modelling, and the latter approach faces with highly complex optimization problems that can only be solved for suboptimal solutions using heuristic or meta-heuristic algorithms [24].

A number of model-based signal control studies that address oversaturated traffic conditions employ the store-and-forward queuing theory traffic model. Gazis [31] followed by [32] designed bang-bang control algorithms to minimize the delay at a two-phase intersection, adopting a queuing theory-based continuous-time traffic flow model. They used a graphical approach to find the optimum switching point between the minimum and maximum green-time allocation to each phase in a way that the residual queues at both approaches dissolve simultaneously. Using the Hamiltonian optimization paradigm, Chang and Sun [33] proposed a discrete-time bang-bang signal control framework by building a state-space model for the queue size dynamics and minimizing a mixed total delay and number of stops objective.

Another cohort of control policies have employed the state-space models built from the queuing theory to design advanced control algorithms for the QD oversaturated periods [34], [35], [36], [37], [38]. [35] proposed the traffic-responsive urban control (TUC) strategy that exploits linear quadratic control techniques to regulate the fixed-cycle phase splits at intersections in a network, while offsets are optimized using a different methodology. Aboudolas *et al.* [34] added a rolling horizon predictive feature to the TUC strategy that leads to efficiency improvements. However, the queuing theory is inaccurate in estimating the spatial queue lengths and the delay at the intersection during oversaturated conditions (see e.g. [16], [39]). In addition to that, the state-space control policies in the form that have been presented in the literature have disadvantages such as: (i) fixing the cycle time that removes a degree of freedom in the decision variable space, (ii) enforcing high computational burdens due to running the optimization every infinitesimal time step, (iii) inability to minimize the total delay at the intersection, and (iv) failing to dictate the undersaturation and queue spillback avoidance constraints.

An alternative traffic model can be derived governed by the LWR theory [40] that enables simultaneous modelling of spatial and temporal coordinates of the queues at the intersection. The estimated total delay from this model is accurate under deterministic traffic settings, as it agrees with the seminal Webster's deterministic delay formula [41]. The LWR theory through modelling shockwaves enables an extra layer to the intersection control to prevent spillbacks. Avoiding the spillback occurrence must be dictated as an essential criterion for any signal control paradigm. Spillback becomes more troublesome for oversaturated intersections, particularly in the QF regimes, as it can quickly spread throughout the network like a disease [42]. Ramezani *et al.* [43] proposed a feedback control algorithm to avoid queue spillovers by identifying congested link pockets along the arterial and minimizing the inflow and maximizing the outflow of those links. Ma *et al.* [44] proposed a multi-stage stochastic optimization algorithm using shockwave theory-based models for the coordinated adaptive control of a series of fixed-cycle intersections.

C. Paper Contributions

Given the predicted time-varying demand profiles, we first propose an analytical traffic flow model based on the shockwave theory. This model captures the queue location dynamics and the vehicle delay of each major movement per cycle, over multiple cycles with time-varying duration, at a generic multi-phase oversaturated intersection throughout the oversaturation period. Thereafter, the FASC algorithm is introduced, which is a model-based discrete-time and proactive signal control policy for oversaturated traffic regimes. The control algorithm employs (i) the predicted arrival flow of each major movement at the intersection and (ii) the proposed traffic flow model in a recursive scheme to instantly obtain the optimal cycle times and phase splits over the whole queue formation and discharging traffic regimes. The operational and spillback avoidance constraints are modelled and enforced in form of linear inequalities. Moreover, an iterative mechanism is embedded into the FASC algorithm to adjust the duration and green-time split of each cycle based on the predicted time-varying demand. The aim of the signal control algorithm is to minimize the total delay at the intersection, while a mixed delay and probability of spillback objective function is additionally introduced for the QF congestion period.

As such, the main contributions of the paper can be summarized as follows: (i) the systematic analytical modelling of the cycle-by-cycle queue location dynamics and delay of major movements at a generic multi-phase signalized intersection over multiple dynamic cycles. (ii) Proposing the FASC algorithm as an efficient, adaptive, and N-stage dynamic cycle-length signal controller that optimizes the vehicle delay and minimizes the spillback occurrence probability at the intersection. And (iii) conducting microsimulation experiments to investigate the performance of the FASC algorithm under different traffic conditions. The accuracy of the traffic flow model is further validated via the microsimulation studies. To add, the effectiveness of the proposed signal control scheme is further compared against (i) optimal fixed-time, (ii) actuated, and (iii) capacity-aware max-pressure (CMP) benchmark algorithms in the microsimulation environment. The results show 63%, 55%, and 40% improvement in the total delay against the fixed-time, actuated, and CMP signal control schemes by using the FASC algorithm.

D. Structure of the Paper

The traffic flow model and signal optimization problem for the QD and QF periods are developed in Sections II-A and II-B, respectively. The FASC method is introduced in Section II-C. Microsimulation experiments are presented in Section III. Finally, the paper is summarized and a few future lines of research are outlined in Section IV.

II. Signal Control for Oversaturated Intersections

This section introduces the Future demand based Adaptive Signal Control (FASC) method. The control algorithm is model-based and tackles both queue formation (QF) and queue discharging (QD) oversaturated periods. During the morning or afternoon rush hours, an intersection's cumulative queue sizes grow during the QF period, and thereafter they dissipate during the QD period. The key idea of the FASC algorithm is to use the predicted demand at the intersection at the beginning of the QF and QD periods, to instantly obtain the optimal signal timings of each phase (i.e. varying cycle times and phase splits). The predicted demand can be time-varying and aggregated (e.g. 5 minute intervals), resulting in a piece-wise constant profile for each movement. This assumption is compelling due to the slow-varying nature of traffic.

An intersection is comprised of two or higher number of *approaches* (also known as an intersection's leg that is used

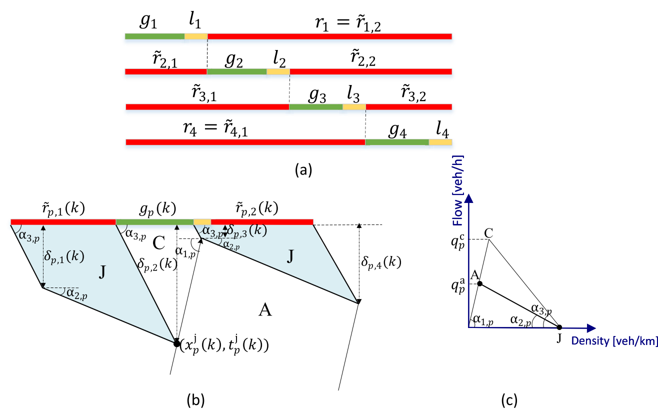

Fig. 1. (a) The effective green time, loss time and red time of the phases of a 4-phase intersection. It is assumed that each cycle starts with the green time in Phase 1 and the green time is sequentially allocated to the next phases. (b) Shockwaves at an oversaturated intersection in the QD regime. Bold lines demonstrate the shockwaves, and shaded areas, J, indicate the stand-still portion of the time-space diagram that provides an estimation of the total vehicle delay at the intersection. (c) The fundamental diagram of the major movement of Phase p. Point J demonstrates the jam state, and Points A and C represent the arrival and saturation states, respectively. These states are highlighted in part (b) of the figure as well.

by the approaching traffic). Each approach is comprised of one or multiple *movements* (a permitted direction of traffic, e.g., straight, left turn, right turn, or a combined movement). A *phase* (or signal phase) is a part of the cycle-time allocated to any combination of non-conflicting movements receiving the right-of-way simultaneously, and a *cycle* (or cycle time) is the time needed for a complete sequence of signal phases. In this paper, a generic isolated multi-approach intersection with P phases is considered, where each phase serves one major (or critical) movement. Without loss of generality, we assume the green times are sequentially allocated based on the phase numbers, i.e. Phase 1 movements receive the green time at the beginning of the cycle and Phase P is the last phase that receives the green time (see Fig. 1a). Furthermore, the following assumptions are considered: [A1] constant saturation flow rates and loss times; [A2] constant arrival flows of the major movements *during each cycle* (the flow rates can vary cycle-by-cycle); [A3] triangular fundamental diagrams; [A4] predictable demand for each major movement throughout the oversaturation period; [A5] allocating only a single green time to each major movement in a cycle; and [A6] the major movement of a phase does not change over time. Assumptions [A1-A3] are commonly adopted in the literature and practice (e.g. [15], [16], [33], [35], [39], [43]). Assumption [A4] can be facilitated using advanced statistical machine learning and deep learning algorithms (see e.g. [45], [46]). Assumptions [A5] and [A6] are implied by the traffic flow modelling proposed in the paper (see Fig. 1a). Assumption [A5] can be satisfied with proper allocation of movements to phases. Note that the FASC algorithm do *not* alter phases (i.e., association of movements to phases) or the sequence of phases in a cycle.

Remark 1: Note that the predicted arrival flow rate of a movement may fluctuate within a cycle. As such, a time-weighted average demand for the cycle duration is calculated to determine the average arrival flow rates of the major movements.

We associate Phase p in cycle k with three time slots: (i) the effective red time $\tilde{r}_{p,1}(k)$ before the start of the effective green time (k is the cycle number); (ii) the effective green time $g_p(k)$; and (iii) the effective red time $\tilde{r}_{p,2}(k)$ after the green time. It is clear that for Phases 1 and P we have $\tilde{r}_{1,1}(k) = 0$ and $\tilde{r}_{P,2}(k) = l_P$. It can be shown that $\tilde{r}_{p,1}(k) = \sum_{j=1}^{p-1} g_j(k) + l_j$, $\tilde{r}_{p,2}(k) = \sum_{j=p+1}^{P} g_j(k) + l_j + l_p$, and $\tilde{r}_p(k) = \sum_{j=1}^{P} g_j(k) - g_p(k) + L$, where l_p is the loss time of Phase p, L is the total loss time at the intersection, and $\tilde{r}_p(k)$ is the effective red time of Phase p. Note that $g_p(k)$ includes the portion of yellow time that is treated as green. To add, loss time l_p takes into account the driver's reaction time and deceleration/acceleration loss times of the approaches served in Phase p.

The traffic flow model and constrained optimization problems for the QD and QF oversturated traffic conditions are discussed in the following sections, followed by the FASC algorithm (Section II-C). Note that the first and second stages of the FASC algorithm are to treat the QF and QD periods, respectively.

A. Signal Optimization for Queue Discharging (QD) Period

In the QD period, while residual queues persist the heavy demand has declined in a way that the intersection fulfills the necessary undersaturation traffic condition [31] demonstrated as

$$\sum_{p=1}^{P} \frac{q_p^{\mathrm{a}}}{q_p^{\mathrm{c}}} + \frac{L}{c^{\max}} \le 1, \tag{1}$$

where q_p^{a} and q_p^{c} are the arrival and saturation flows of the major movement of Phase p, and $c^{\max}$ is the maximum admissible cycle length at the intersection. It is assumed that the time-varying arrival flows at the intersection are predicted. Accordingly, the start of the QD period is when the predicted demand q_p^{a} satisfies Condition (1). Note that, the residual queues accumulated through the queue formation (QF) period need to be cleared during QD period and thus the intersection is still oversaturated. The control algorithm aims to discharge the residual queues in exactly N cycle-times. Accordingly, an adaptive N-stage discrete signal optimization algorithm to determine the optimal cycle lengths and phase splits is established in this section. In light of that, the traffic flow dynamics is built on the principles of the shockwave (LWR) theory.

The derivation of the fundamental characteristics of the traffic flow for an *undersaturated* signalized intersection using the principles of the shockwave theory have been extensively studied in the literature (e.g. [40], [47], [48], [49]). The LWR theory accurately estimates the total delay at the intersection when the traffic complies with Assumptions [A1-A4] [2], [16]. Fig. 1b demonstrates the traffic shockwaves of the major movement served in Phase $p \in \{1, \ldots, P\}$, in accordance with the fundamental diagram (FD) of the approach depicted in Fig. 1c.

It is assumed that every residual queue should be fully discharged in the Nth cycle or prior to that, and the timing of each phase in cycle k can be split into $\tilde{r}_{p,1}(k)$, $\tilde{r}_{p,2}(k)$, and $g_p(k)$. To calculate the total vehicle delay per cycle it is crucial to estimate the queue lengths $\delta_{p,i}(k)$, $i \in \{1, \ldots, 4\}$. The total delay of Phase p in a cycle is the shaded area depicted in Fig. 1b (representing the jam state of traffic) multiplied by the jam density of the critical movement of the phase. From the FD characteristics, the following equations are derived:

$$\delta_{p,1}(k) = \delta_{p,4}(k-1), \tag{2a}$$
$$\delta_{p,2}(k) = \delta_{p,1}(k) + \Gamma_p(k)\tilde{r}_{p,1}(k), \tag{2b}$$
$$\delta_{p,3}(k) = \delta_{p,2}(k) - q_p^{\mathrm{c}}/\kappa_p^{\mathrm{jam}} g_p(k), \tag{2c}$$
$$\delta_{p,4}(k) = \delta_{p,3}(k) + \Gamma_p(k)\tilde{r}_{p,2}(k), \tag{2d}$$

wherein $\Gamma_p(k) \triangleq q_p^{\mathrm{a}}(k) q_p^{\mathrm{c}} / \left((q_p^{\mathrm{c}} - q_p^{\mathrm{a}}(k)) \kappa_p^{\mathrm{jam}} \right)$ is the speed of shockwave between arrival and jam densities, and κ_p^{jam} is the jam density of the major movement in Phase p and cycle k. To add, the maximum queue length in Phase p and cycle k reads as

$$x_p^{\mathrm{j}}(k) = \max\left(\delta_{p,2}(k), \delta_{p,4}(k)\right). \tag{3}$$

Total vehicle delay of the major movements at the intersection throughout the queue discharging period reads as

$$D_{\mathrm{T}}^{N} = \sum_{k=1}^{N} \sum_{p=1}^{P} D_p(k), \tag{4}$$

where $D_p(k)$ is the total delay of the major movement of Phase p in Cycle k that can be formulated as:

$$\begin{aligned} 1/\kappa_p^{\mathrm{jam}} D_p(k) = {} & \left(\delta_{p,1}(k) + 0.5\Delta\delta_{p,1}(k)\right)\tilde{r}_{p,1}(k) \\ & + \left(\delta_{p,3}(k) + 0.5\Delta\delta_{p,3}(k)\right)\tilde{r}_{p,2}(k), \end{aligned} \tag{5}$$

and $\Delta\delta_{p,i}(k) = |\delta_{p,i+1}(k) - \delta_{p,i}(k)|$, $i = \{1, 3\}$.

The following constraints should be realized to: (i) discharge the residual queues (i.e. $\delta_{p,3}(k)$) within N cycles without pushing them to be cleared simultaneously (Conditions (6b) and (6d)), (ii) prevent the queue sizes to grow in subsequent cycles (Condition (6c)), and (iii) employ the full capacity of the intersection in clearing the congestion implied by Condition (6a) ($k = \{1, \ldots, N-1\}$ and $p \in \{1, \ldots, P\}$):

$$\delta_{p,3}(k) \ge 0, \tag{6a}$$
$$\sum_{p=1}^{P} \delta_{p,3}(k) > 0, \tag{6b}$$
$$\delta_{p,3}(k) \ge \delta_{p,3}(k+1), \tag{6c}$$
$$\delta_{p,3}(N) = 0. \tag{6d}$$

To add, the minimum green time to account for pedestrians, and the maximum operational cycle length requirements can be implied by

$$g_p(k) \ge g_p^{\min} \quad p \in \{1, \ldots, P\},\ k \in \{1, \ldots, N\}, \tag{7a}$$
$$\sum_{p=1}^{P} g_p(k) + L \le c^{\max} \quad k \in \{1, \ldots, N\}. \tag{7b}$$

Furthermore, the following inequality governs the undersaturation property at the intersection when *ignoring* the residual queues ($p \in \{1, \ldots, P\}, k \in \{1, \ldots, N\}$) [16]:

$$(1 - \eta_p(k) - \frac{1}{P-1})\left(\sum_{j=1}^{P} g_j(k) + L\right) + (\eta_p(k) + \frac{1}{P-1})g_p(k) + \frac{2-P}{P-1}l_p \geq 0, \quad (8)$$

wherein $\eta_p(k) \triangleq q_p^{\mathrm{a}}(k)/\left(q_p^{\mathrm{c}} - q_p^{\mathrm{a}}(k)\right)$. The inequality explains that the current cycle's demand has to be addressed within the cycle and thus no additional residual queues are generated.

The spillback avoidance constraint is dictated as

$$x_p^{\mathrm{j}}(k) \leq \beta_p \Delta_p \quad k \in \{1, \ldots, N\}, \;\; p \in \{1, \ldots, P\}, \quad (9)$$

where $\beta_p \geq 1$ is a weighting coefficient indicating the phase priority for enforcing the constraint, such that greater β_p indicates a lower priority of spillback avoidance in Phase p. The queue clearance point for the first and last phases are $x_1^{\mathrm{j}}(k) = \delta_{1,4}(k)$ and $x_P^{\mathrm{j}}(k) = \delta_{P,2}(k)$. To formulate the constraint in a more convenient style, we assert from (3) and (9) that $\delta_{p,2} \leq \beta_p \Delta_p$ for $p \in \{2, \ldots, P\}$, and $\delta_{p,4} \leq \beta_p \Delta_p$ for $p \in \{1, \ldots, P-1\}$.

Remark 2: Note that the delay of the minor movements of each phase are excluded in (4), since (i) they have lower priority to be optimized, and (ii) movement's delay formula (5) and Constraint (6)(a) may not necessarily hold for the minor movements during a cycle. The latter implies excessive complexities to the mathematical modelling of the objective function. To reflect the importance of minor movements in the delay optimization objective function, we weight the delay of each major movement in (4) by a user-defined constant $\chi_P \geq 1$, and define a modified delay objective function as follows:

$$DO_{\mathrm{T}}^{N} = \sum_{k=1}^{N}\sum_{p=1}^{P} \chi_p D_p(k). \quad (10)$$

Hyper-parameters χ_p are specified based on (i) the structure of the intersection, (ii) the number of movements of the phase and (iii) the level of congestion of the minor movements.

Remark 3: In the queue discharging period, β_p can be fixed at $\beta_p = 1$ to avoid spillback at every movement, unless if the residual queues are close to the end of the critical links, and spillback at one or multiple movements are unavoidable. However, in the QF period, as demonstrated in Section III via microsimulation studies, it is often inevitable to observe spillback at one or multiple movements due to the long time heavy demand at the intersection and low storage capacity of the links. Therefore, the role of β_p parameters become more crucial in protecting critical movements at the intersection, e.g. the movements that serve the major corridor.

The derived delay objective function (10) can be written in the quadratic form below

$$DO_{\mathrm{T}}^{N}(\Theta_N) = \Theta_N^T \mathbf{A_N} \Theta_N + \mathbf{B_N}^T \Theta_N + \mathbf{C_N}, \quad (11)$$

where $\Theta_N = [G(1); \ldots; G(N)]$, and $G(k) = [g_1(k); \ldots; g_P(k)]$, $k \in \{1, \ldots, N\}$, $\mathbf{A_N}$, $\mathbf{B_N}$, and $\mathbf{C_N}$ are matrices defined in Appendix A-A. Constraints (6) are linear in decision variables $g_p(k)$, and can be expressed in the following closed linear forms ($k \in \{1, \ldots, N-1\}$ and $p \in \{1, \ldots, P\}$):

$$H_{p,1}^{k}\Theta_N \geq b_{p,1}^{k}, \quad (12a)$$
$$H_{p,2}^{k}\Theta_N > b_{p,2}^{k}, \quad (12b)$$
$$H_{p,3}^{k}\Theta_N \geq b_{p,3}^{k}, \quad (12c)$$
$$H_{p,1}^{N}\Theta_N = b_{p,1}^{N}, \quad (12d)$$

where $H_{p,1}^{k}$, $H_{p,2}^{k}$, and $H_{p,3}^{k}$ are $1 \times NP$ matrices, and $b_{p,1}^{k}$, $b_{p,2}^{k}$, and $b_{p,3}^{k}$ are scalar parameters that are elaborated in Appendix A-B. Moreover, operational constraints (7) can be formulated as

$$\Theta_N \geq \Theta_N^{\min}, \quad (13a)$$
$$H_4^k \Theta_N \geq b_4 \quad k \in \{1, \ldots, N\}, \quad (13b)$$

where $\Theta_N^{\min} = \left[G^{\min}; \ldots; G^{\min}\right] \in \mathbb{R}^{NP\times 1}$, $G^{\min} = \left[g_1^{\min}; \ldots; g_P^{\min}\right] \in \mathbb{R}^{P\times 1}$, $H_4^k = \left[\mathbf{0}_{(k-1)P}, -\mathbf{1}_P, \mathbf{0}_{(N-k)P}\right]$, and $b_4 = L - c^{\max}$. Undersaturation constraint (8) can also be written in the following compact form:

$$H_{p,5}^{k}\Theta_N \geq b_{p,5}^{k} \quad k \in \{1, \ldots, N\}, \;\; p \in \{1, \ldots, P\}. \quad (14)$$

To add, the spillback avoidance constraints to imply $\delta_{p,2} \leq \beta_p \Delta_p$ and $\delta_{p,4} \leq \beta_p \Delta_p$ read as:

$$H_{p,6}^{k}\Theta_N \geq b_{p,6}^{k} \quad k \in \{1, \ldots, N\}, \;\; p \in \{2, \ldots, P\}, \quad (15a)$$
$$H_{p,7}^{k}\Theta_N \geq b_{p,7}^{k} \quad k \in \{1, \ldots, N\}, p \in \{1, \ldots, P-1\}, (15b)$$

where the details of (14), (15a), and (15b) are given in Appendix A-B.

Using the developed analytical formulations and Assumption [A4], the optimal green times at the intersection can be obtained via solving the following optimization program:

$$\underset{g_p(k),\quad k=\{1,\ldots,N\},\;\; p=\{1,\ldots,P\}}{\text{minimize}} \quad \mathbf{O_N}(g_p(k)),$$
$$\text{Subject to: (12), (13), (14), and (15)} \quad (O_{qd})$$

where $\mathbf{O_N}(g_p(k))$ is the objective function (considering N cycles), which is the total delay (11). Problem (O_{qd}) is a quadratic non-convex program, as $\mathbf{A_N}$ is often indefinite. However, global optimal solutions can be sought for this class of optimization problems using advanced numerical methods (see e.g. [50], [51]).

Remark 4: Note that the undersaturation constraint (8) and the spillback avoidance constraint (9) can be in conflict under special circumstances, such as short link length of one movement. In such occasions, the undersaturation constraint can be undermined since the intersection is already oversaturated and constraints (6) ensure that the residual queues are non-increasing.

B. Signal Optimization for the Queue Formation (QF) Period

Queue formation regime represents the duration when the overall arrival flow are higher than the intersection's capacity and the undersaturation condition does not hold. Therefore, the residual queue lengths at one or multiple movements start to increase. Let us assume this period lingers τ hours and N cycles is devoted to this period. The FASC strategy treats this problem with the objective of (i) minimizing the total delay, or (ii) minimizing a mixed total delay and probability of spillback function at the intersection within this period, as well as preventing the spillback phenomenon at one or multiple movements.

The queue length dynamics and cumulative total delay of major movements at the intersection can be readily estimated from our developed models (2) and (11), respectively. It is clear that the undersaturation constraint and Constraints (6b)-(6d) may not hold during this period. However, the non-negative residual queue length and spillback avoidance constraints (i.e. (6a) and (9)) should still be satisfied. Moreover, the following constraint indicates that the period lasts for at least τ unit of time:

$$\mathbf{1_{NP}}^T \Theta_N \geq \tau - NL. \tag{16}$$

It is clear that N must be sufficiently large so that $\tau/N \leq c^{\max}$. Hence, the optimization problem reads:

$$\begin{aligned} &\underset{g_p(k),\quad k=\{1,\ldots,N\},\ p=\{1,\ldots,P\}}{\text{minimize}} \quad \mathbf{O_N}(g_p(k)), \\ &\qquad \text{Subject to: (13), (12a), (15), and (16)} \qquad (O_{qf}) \end{aligned}$$

where $\mathbf{O_N}(g_p(k))$ represents the delay objective function (11).

Remark 5: Note that due to the stochastic nature of demand profile, the undersaturation constraint might be valid for a few cycles within the QF period. For instance, the intersection may first experience 10 minutes of intensive arrival demand, then 5 minutes of medium arrival flows, followed by another duration of high demand. The whole duration that we expect high intensity arrival flows is classified as the QF period and optimization program (O_{qf}) is applied to work out the optimal signal timings. Comparing (O_{qd}) and (O_{qf}), the optimization problems for the queue formation and discharging periods are only different in their constraints. The non-negative queue length, spillback avoidance, and operational constraints from (O_{qd}) are enforced and constraint (16) is added.

Although optimization problem (O_{qf}) accounts for spillback avoidance as a constraint, the objective function is not sensitive to the probability of spillback. This could be problematic during the queue formation period. In particular, for an asymmetric intersection minimizing the vehicles delay can be against balancing the queue lengths at reasonable levels, which leads to the spillback of one or multiple movements. Hence, the below modified objective function mixing the total delay and the probability of spillback is defined:

$$\begin{aligned} &DS_{\mathrm{T}}^{N}(\Theta_N) = \omega_1 DO_{\mathrm{T}}^{N}(\Theta_N) \\ &+0.5\omega_2 \sum_{k=1}^{N}\sum_{p=1}^{P}\left(\frac{\epsilon_p}{\alpha_p\Delta_p - \delta_{p,2}(k)} + \frac{\epsilon_p}{\alpha_p\Delta_p - \delta_{p,4}(k)}\right), \end{aligned} \tag{17}$$

where $\epsilon_p > 0$, $\omega_i \in (0,1)$, $\sum_{i=1}^{2}\omega_i = 1$, and $\alpha_p \geq \beta_p$ is a link length scaling coefficient. α_p is defined to adjust the sensitivity of the objective function $DS_{\mathrm{T}}^{N}(\Theta_N)$ to the probability of spillback at the major movement served in Phase p. Given that the maximum queue length of each phase is either $\delta_{p,2}(k)$ or $\delta_{p,4}(k)$, the second part of the objective function $DS_{\mathrm{T}}^{N}(\Theta_N)$ reciprocally grows when the maximum queue length approaches the scaled link length $\alpha_p\Delta_p$, which is the threshold of the acceptable queue length. The threshold, which could be greater than the spillback avoidance constraint threshold $\beta_p\Delta_p$, can be appropriately adjusted to be larger than the link length in a heavily congested intersection to find an admissible solution for the signal optimization problem. This guideline should be exercised in scenarios where spillback or near spillover conditions are unavoidable in minor or prevailing road sections. The scenarios include: (i) long congestion periods, (ii) significantly high demand, or (iii) the existence of short links. Moreover, the spillback avoidance constraint should be treated as advised in Remark 3.

Optimization problem (O_{qf}) with $DS_{\mathrm{T}}^{N}(\Theta_N)$ as the objective is a mixed nonlinear program (MNLP) comprising a (non-convex) quadratic function and a nonlinear convex function as the objective. This problem is more intricate than choosing the total delay as the objective, which is a non-convex quadratic program. However, the global optimal solution can be sought applying *spatial branch-and-bound* optimization algorithm as demonstrated in [52] and [53]. Moreover, the local optimal solution can be found using the sequential quadratic programming (SQP) technique. The local optima can be close to the global optima, provided that the feasibility region is adequately tight.

A challenge confronting the implementation of an adaptive (or dynamic) cycle length signal control strategy is estimating the termination time of the QD period and the expected arrival flow of each cycle. This in turn creates inaccuracies in the estimation of the delay and constraint parameters in the optimization problem (O_{qd}). To overcome this challenge, a simple iterative algorithm, named Adaptive Flow Updating (AFU) scheme, is proposed to recursively update the cycle times and thus arrival flow rates of each cycle. The algorithm initializes the cycle times at arbitrary values and accordingly estimates the arrival flows based on the initial cycle times and the predicted arrival flow profiles. Thereafter, depending on the traffic regime (QF, QD, or undersaturated), it recursively solves the optimization algorithm for optimal signal timings, and updates the arrival flows accordingly. The algorithm terminates when the sum of the absolute differences of the arrival flows obtained from the current and the previous steps along the rolling horizon is less than a sufficiently small threshold, which indicates a steady-state condition.

C. The FASC Algorithm

In this section, the complete FASC algorithm is presented. In summary, at the beginning of the QF congestion period, the algorithm seeks the optimal number of cycles and signal timing for the whole QF period based on the predicted demand profile of each movement. After the QF period and at the start of the QD period, the algorithm delves the optimal signal

Arrival Flow Updating (AFU) Algorithm

I. Initiate arrival flow rates $q_p^{\mathrm{a}}(i) = 0$ and cycle lengths c(i) $(i \in \{1, \cdots, N\},\ p \in \{1, \cdots, P\})$

II. Based on the predicted demand profile and given initial $c(i)$, estimate the expected arrival flow rate per cycle $q_p^{\mathrm{a,new}}(i)$

while $\sum_{i=1}^{N} \sum_{p=1}^{P} |q_p^{\mathrm{a,new}}(i) - q_p^{\mathrm{a}}(i)| > q^{\mathrm{Th}}$ **do**

% q^{Th} is the error threshold in the norm of the updated arrival flow rate with respect to the flow rates of the previous iteration.

if Queue formation (QF) period **then**

III. Calculate $\mathbf{A_N}$, $\mathbf{B_N}$, $\mathbf{C_N}$, $H_{p,j}^{i}$ $(j \in \{1, 4, 6, 7\})$

IV. Solve program (O_{qf})

else if Queue discharging (QD) period **then**

III. Calculate $\mathbf{A_N}$, $\mathbf{B_N}$, $\mathbf{C_N}$, $H_{p,j}^{i}$ $(j \in \{1, \cdots, 7\})$

IV. Solve program (O_{qd})

end if

Output: $\Theta_N^{\mathrm{opt,new}} \rightarrow c^{\mathrm{new}}(i)$

V. $q_p^{\mathrm{a}}(i) \leftarrow q_p^{\mathrm{a,new}}(i)$

VI. Given $c^{\mathrm{new}}(i)$, estimate the new arrival flow rates $q_p^{\mathrm{a,new}}(i)$

end while

timings to discharge the queues in the desirable number of cycles. Therefore, in the current form of the FASC algorithm, numerical optimizations are only run twice throughout the congestion period, which is numerically highly efficient. The pseudo-code of the algorithm is given below.

Number of cycles to discharge the queues in the QD traffic regime (problem (O_{qd})) or to accommodate the queues in the QF period (problem (O_{qf})) is a hyper-parameter that needs to be adjusted appropriately. This can be addressed by an iterative scheme integrated into the FASC algorithm in each congestion regime. However, our experiments emphasize that the smallest admissible N normally results in the best performance of the algorithm in terms of minimizing the objective function.

Remark 6: A simple variation of FASC control paradigm is to update the signal timings every certain time interval τ^{u}, i.e. repeating Steps III-VI in the QF period and Steps III-VII in the QD period. In light of that, the demand prediction algorithm updates the forecasted demand profiles based on the real-time feedback from loop detectors, and thus Program (O_{qd}) (for QF period) or Program (O_{qd}) (for QD period) is rerun at the end of every τ^{u} time-interval to readjust the signal settings based on the updated information for the rest of the congestion period. By adopting this variation, the control algorithm becomes a rolling horizon control paradigm with time-varying cycle lengths. Studying the impacts of this modification on reducing congestion and on computational complexities is a subject for future research.

FASC Algorithm

I. Measure the initial queue lengths $\delta_{p,1}(1)$ $(p \in \{1, \cdots, P\})$

II. Predict the arrival flow rates, $q_p^{\mathrm{a}}(t)$, at the intersection for sufficient number of time-steps ahead

% Arrival flow at each time-step (e.g. 5 minute intervals) represents the expected average demand during that time-step

if Queue formation (QF) period **then**

III. Define the objective function and set $\mathcal{N}$

% objective function can be chosen from: (a) total delay, and (b) mixed total delay and probability of spillback. $\mathcal{N}$ is the set of nominal number of cycles to be allocated to the QF period.

for $N = \mathcal{N}$ **do**

IV. Initiate $c(i) = \tau/N,\ i \in \{1, \cdots, N\}$

% τ is the expected duration of QF period.

V. Apply the AFU algorithm

Output: Θ_N^{opt}

end for

VI. Choose N^{opt} and thus $\Theta_{N^{\mathrm{opt}}}^{\mathrm{opt}}$ in the set of admissible $N \in \mathcal{N}$

% Criteria of choosing the optimal N could be minimizing the objective function, or its variability per cycle.

else if Queue discharging (QD) period **then**

III. Define $\mathcal{N}$ the set of nominal number of cycles to discharge the residual queues

for $N = \mathcal{N}$ **do**

IV. Initiate $c(i) = c^{\max},\ i \in \{1, \cdots, N\}$

V. Apply the AFU algorithm

Output: Θ_N^{opt}

end for

VI. Choose N^{opt} and thus $\Theta_{N^{\mathrm{opt}}}^{\mathrm{opt}}$ in the set of admissible $N \in \mathcal{N}$

% Criteria for choosing the optimal N could be minimizing the objective function, or its variability per cycle.

end if

III. Microsimulation Experiments

The intersection of Victoria road and Terry street, a key intersection on the Victoria corridor connecting CBD and northern suburbs of Sydney metropolitan area, is considered for microsimulation studies. The intersection is modelled and calibrated in Aimsun environment (see Fig. 2). The signalized intersection comprises 3 approaches and 5 movements with two major movements: (i) through movement of Link 42455 (Victoria road) and (ii) left turn of Link 29244 (Terry street). The intersection is controlled with a two-phase plan as shown in Fig. 2. There is one bus lane on the inbound direction of Victoria road (see Fig. 2) that is shared with the left turning vehicles. Therefore, Movements 1 and 2 have three and two effective lanes, respectively. However, the second movement's link length (346 [m]) is dominated by a single lane, with the last 60 meters assisted by a turn bay. Thus, it is considered as a single-lane link for jam density estimation and a two-lane link for saturation flow estimation. Only passenger vehicles are considered in this study, thus the pedestrian movements and phases are excluded. Traffic flow characteristics of the roads measured via field experiments are shown in Table I. The tests consider the morning rush period, 8:00 am to 9:45 am.

We first examine the accuracy of the proposed LWR theory-based traffic flow model against the microsimulation model with a time-varying demand similar to the field demand

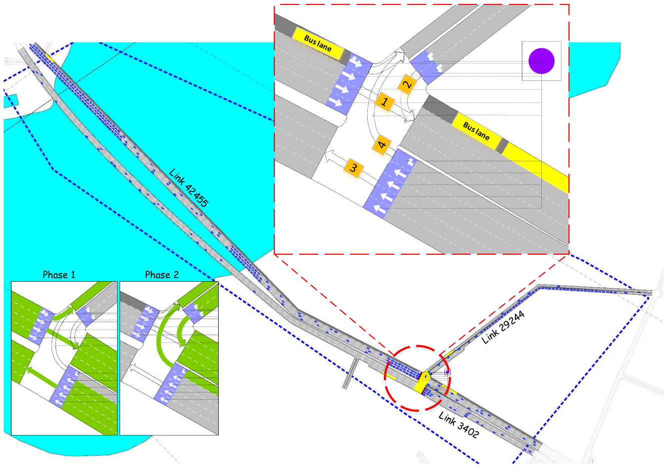

Fig. 2. Microsimulation model of the intersection of Victoria road and Terry street in Sydney. The intersection has 3 approaches, 5 movements, and 2 phases. Link 42455 contains a bus lane that is shared by the left-turning vehicles. Movements 1 and 2 highlighted in the figure are the major movements of Phases 1 and 2, respectively. Moreover, the movements in each phase are exclusively depicted. Vehicles are shown by blue dots on the roads, and the figure shows that Links 42455 and 29244 can become heavily congested and experience queue spillover.

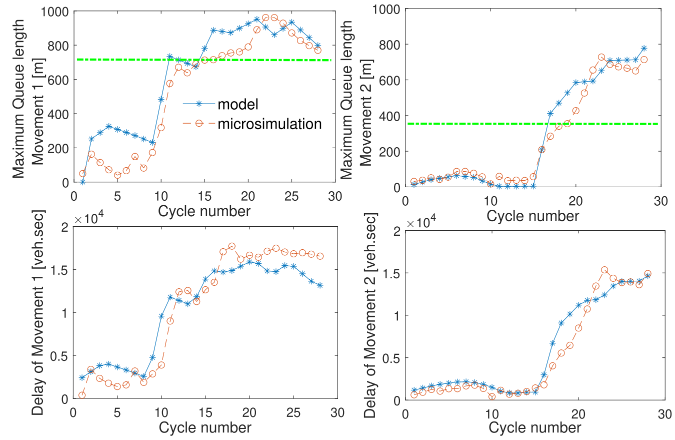

Fig. 4. Maximum queue length (top figures) and total vehicle delay (bottom figures) per cycle for Movements 1 and 2 at the simulated intersection, comparing the developed mathematical model and average results of 5 microsimulation replications with different random seeds. The QF period, which is the first 30 cycles (120 [s]) of simulation are considered for this experiment. The link length of each movement is highlighted by a dashed-dot green line in the top figures, indicating that queue spillover is observed at both movements, which is accurately captured by the proposed traffic model. The additional queue length of a movement in microsimulations is estimated via measuring the virtual queue lengths.

TABLE I

TRAFFIC FLOW CHARACTERISTICS AND OPERATIONAL PARAMETERS OF THE MAJOR MOVEMENTS AT THE INTERSECTION IN THE MICROSIMULATION STUDY

Movement	q_i^c[veh/h]	κ_i^c[veh/km]	κ_i^j[veh/km]	$g_i^{\min}$[s]	l_i[s]	$d_i(0)$[veh]	Δ_i[m]
1	4500	75	540	10	4.2	9	708
2	3000	60	180	5	4.2	0	346

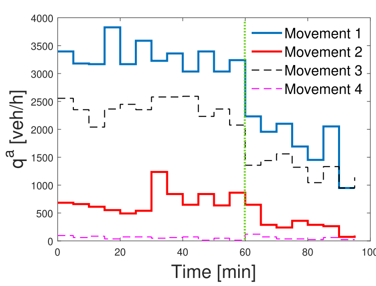

Fig. 3. Arrival flow demand of each movement at the simulated intersection. The flows are aggregated in 5-minute intervals. Movements 1 and 2 are the critical movements of Phases 1 and 2. The intersection is in the QF period in the first hour, and it is in the QD period thereafter. The two periods are segregated via a dashed green line.

during the studied period. The demand is aggregated into 5-minute intervals as demonstrated in Fig. 3. The intersection is in the queue-formation period in the first hour of simulation, and thereafter the demand drops to the undersaturation traffic regime. This demand is used for evaluation of the developed traffic flow model for oversaturated periods, and 110% of the demand is applied at the intersection for evaluating the FASC algorithm's performance.

A. Validation of the Traffic Flow Model

For evaluating the accuracy of the proposed traffic flow model in estimating the delay and maximum queue length at the intersection (see Section II-A), we set up a pre-timed signal plan with fix cycle time of $c = 120$ [s]. Taking the average demand of each movement throughout the simulation, the optimal fixed green time plus loss time of Phases 1 and 2 are obtained as 93 [s] and 27 [s], respectively. The arrival flows were assumed to be stochastic and follow an exponential distribution. To add, the yellow time at the intersection is set at 3 seconds for each phase. However, the actual loss-time of each movement is slightly higher to account for the acceleration/deceleration of vehicles.

A microsimulation API were developed to measure the accurate maximum queue length and total vehicle delay of each movement per cycle. Total delay of a road section in each cycle is estimated by measuring the delay of every vehicle that exit the section, plus the delay accumulated by the vehicles in the *virtual queue*. Virtual queue corresponds to vehicles that are stacked outside the link and are awaiting to enter the section due to the spillback phenomena.

The average maximum queue length and delay of each major movement were attained from running the microsimulation model for the first hour of the experiment (30 cycles). Five different random replications are compared against the results obtained from the developed model (Equations (2) and (5)) in Fig. 4. Note that the first hour of simulation corresponds to the queue formation period. Moreover, the queue lengths shown in figure 4 represent the maximum queue length plus the virtual queue length, whenever the major movement is suffering from spillback phenomena. The link length of each major movement is depicted via a dashed green line. It is clear that both movements experience the spillback phenomena and the proposed model effectively capture it. The Mean Absolute Errors (MAEs) for the maximum queue length and delay of each movement are reported in Table II. The results emphasize an acceptable accuracy of the mathematical models (11) and (3) in estimating the delay and maximum queue length of

TABLE II
MAE OF THE ESTIMATED MAXIMUM QUEUE LENGTH AND DELAY OF EACH MOVEMENT COMPARED AGAINST THE MICROSIMULATION STUDIES

	Movement 1	Movement 2
Maximum queue length [m]	109	48
Vehicle delay [veh.min]	30	16

each movement, despite the stochasticity implied intrinsically by the microsimulation environment (e.g. stochastic arrival and departure flows, different acceleration and deceleration values, and stop-and-go waves in the simulated traffic environment).

B. Signal Control Experiments and Results

Four signal control policies are implemented and compared using a demand with 10% higher intensity than Fig. 3: (i) fixed, (ii) actuated, (iii) capacity-aware max-pressure (CMP), and (iv) the proposed FASC method. The fixed signal control uses the fixed cycle time and green time splits as described in Section III-A (93 [s] and 27 [s] for green plus loss times of Phases 1 and 2, respectively). In the actuated signal control algorithm the maximum green-time of each major movement is equal to the green times of the fixed control scheme, and the minimum green time of Phases 1 and 2 are 71 [s] and 17 [s], respectively.

The CMP algorithm [28] is an advanced max-pressure signal control method [27] that accounts for the vehicle capacity of road segments. The algorithm is primarily developed for a network of intersections, but it can also be applied to an isolated intersection. Hence, it is considered as a benchmark method in our study. For an isolated intersection, the algorithm updates the activated phase every time-step t_s (we assume $t_s = 5$ [sec] in this study), to maximize the normalized pressure relief at the intersection. The normalized pressure of phase p at time t is defined as $P_p(t) \triangleq \sum_{i\in\phi(p)}(\lambda_i(t)/C_i)q_i^c$, where $\lambda_i(t)$ is the number of vehicles of Movement i at time t, C_i is the maximum number of vehicles that Movement i can accommodate, and $\phi(p)$ is the set of movements that get the right-of-way in Phase p.

Given that the implemented demand at the intersection is 10% more severe than the pictured demand in Fig. 3, the intersection is in the QF oversaturated traffic regime for the first 1-hour of the simulation (according to the condition outlined in Inequality (1)). Note that the oversaturation condition does not necessarily hold throughout the queue-formation period, though it is the dominant condition for most of the 1-hr period. Thereafter, by declining the demand at the intersection, traffic switches to the QD oversaturated regime followed by the undersaturated condition.

The proposed signal control strategy was implemented for minimizing the total delay objective (10) at the intersection, first for the queue-formation and next for the queue-discharging traffic regimes. Note that the FASC algorithm is conducted only one time at the beginning of the QF (the beginning of simulation) and one time at the beginning of the QD (after 1 hour of simulation) periods. The FASC algorithm only took *240* [ms] and *30* [ms] to find the optimal signal timings for the QF and QD regimes, respectively. The

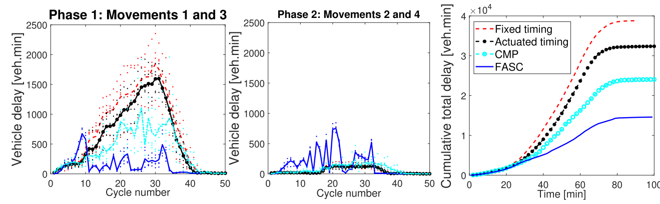

Fig. 5. Total vehicle delay results from implementing the proposed FASC, capacity-aware max pressure (CMP), the fixed-time and actuated signal control methods. The results of microsimulation replications are depicted by dot points, and the average results are shown by distinguished line styles with the same colors as the corresponding dot points.

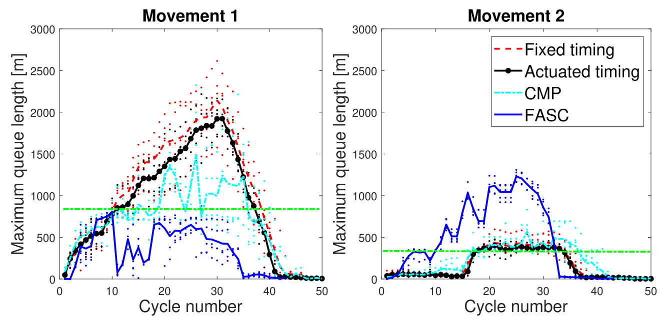

Fig. 6. Maximum queue length results from implementing the proposed FASC, CMP, the fixed-time and actuated signal control methods. The queue lengths per cycle of Movements 1 and 2 are depicted and the link length of each movement is highlighted by a dashed-dot green line. The results of microsimulation replications are depicted by dot points, and the average results are shown by distinguished line styles with the same colors as the corresponding dot points.

maximum cycle length was fixed at $c^{\max} = 240$ [s], and we set $\chi_1 = \chi_2 = 1$. Due to the heavy demand during the QF period, it is not possible to enforce the spillback avoidance at both major movements ($\beta_1 = \beta_2 = 1.0$). Therefore, to enable solving (O_{qf}) and to give higher priority to the movements of Phase 1 that serve the major corridor, we set $\beta_1 = 1$ and $\beta_2 = 5$. This implies that the maximum queue length of Movement 1 should not exceed the link length, whereas the admissible queue length of Movement 2 (which is the minor road) can grow to up to 5 times of the link's length.

The total delay and queue length results of microsimulation experiments (comprising 5 replications) are shown in Figs. 5 and 6, respectively. Cycle-by-cycle total vehicle delays of movements of Phases 1 and 2, together with the cumulative total delay at the intersection over time obtained from the implemented control schemes are exhibited in Fig. 5. It can be seen that by implementing the proposed control scheme the total delay of vehicles in Phase 1 has been substantially improved, while the delay in Phase 2 has grown. The overall total vehicle delay at the intersection has reduced by 63%, 55%, and 40% with respect to the fixed, actuated, and CMP control methods, respectively. Considering the maximum queue lengths in Fig. 6, it is clear that the FASC algorithm effectively suppresses the spillback in Movement 1, and maintains the maximum queue due to the demand of Movement 2 below 1730 [m] that is 5 times the link length. However, the alternative fixed-time and actuated control schemes result in heavy congestion in the major corridor, in a way that the back of the queues have reached 2.5 kilometers from the stop-line at the end of the queue formation period. The max-pressure algorithm has been more effective than the fixed-time and actuated methods in protecting Movement 1 from spillback, though not as effective as the FASC method, due to the high pressure on Movement 2.

IV. Summary and Future Works

The pivotal problem of adaptive traffic signal optimization for an isolated multi-phase oversaturated intersection has been explored covering both queue formation and discharging regimes. Based on the traffic flow characteristics of the major movements, the queue length and the total delay of the major approaches at the intersection have been analytically modelled for the whole oversaturation period, given that the demand of each movement is predicted in a sufficiently large time horizon. The LWR theory has been employed to capture both temporal and spatial dynamics of the queues. Using the developed analytical model, the FASC scheme has been proposed to efficiently find the global optimal signal timings with dynamic cycle lengths and phase splits at the intersection throughout the oversaturation period. The algorithm only runs twice, i.e. at the beginning of the QF and QD periods, to adjust the cycle lengths (with time-varying duration) and phase splits at the intersection. The proposed control method can also be readily implemented in a rolling-horizon structure.

Comprehensive microsimulation experiments on a congested intersection in Sydney have highlighted the superiority of the FASC policy compared to the benchmark optimal fixed-time, actuated, and capacity-aware max-pressure methods.

Multitude of directions can be envisaged for this research. Formulating the optimization problem for multiple *coordinated* intersections is a challenge, particularly for control policies with adaptive cycle lengths. Another indispensable direction is adapting the proposed algorithms to accommodate public transport and connected and automated vehicles (CAVs) by adding extra control layers such as lane management policies [49]. More importantly, feedback control algorithms should be developed to tackle bounded errors in demand prediction that may deteriorate the potential performance of any control schemes. In addition, the FASC algorithm can be integrated into a hierarchical network perimeter control method, as the intersection-level signal controller for the efficient management of the cumulative traffic at the perimeter's intersections.

Appendix A
Traffic Flow Model Parameters

A. Parameters of the Delay Model

This section first describes the quadratic form of the total delay model (11) obtained from the shockwave theory. Matrix $\mathbf{A_N} = \left[A_{k_1k_2}\right]_{NP\times NP} \in \mathbb{S}^{NP\times NP}$ is a symmetric matrix that is established from block matrices $A_{k_1k_2} \in \mathbb{S}^{P\times P}$, $k_1, k_2 \in \{1,\dots,N\}$. The block diagonal matrices A_{kk} are calculated form $A_{kk} = \sum_{p=1}^{P}\chi_p\kappa_p^{\text{jam}}\tilde{A}_p^{kk}$, where $\tilde{A}_p^{kk} = \left[\tilde{A}_p^{kk}(i,j)\right]_{P\times P} \in \mathbb{S}^{P\times P}$. Indeed, $\tilde{A}_p^{k_1k_2}(i,j)$ indicates the multiplier of the term $g_i(k_1)g_j(k_2)$ in the delay model for Phase p.

In a greater detail, for $k < N$ we have $\tilde{A}_p^{kk}(i,j) = 0.5\Gamma_p(k)$, for $i,j \in \{1,\dots,P\}\setminus p$, $\tilde{A}_p^{kk}(i,p) = 0$ for $i \in \{1,\dots,p\}$, and $\tilde{A}_p^{kk}(i,p) = -0.5q_p^{\text{c}}/\kappa_p^{\text{jam}}$, for $i \in \{p+1,\dots,P\}$. Moreover, when $k = N$ it can be shown that since $\delta_{p,3}(N) = 0$, we have $\tilde{A}_p^{NN}(i,j) = 0.5\Gamma_p(N)$ for $i,j \in \{1,\dots,P\}\setminus p$, and $\tilde{A}_p^{NN}(i,j) = 0$ if $i = p$ or $j = p$.

When it comes to the off-diagonal blocks, let us assume $k_1 < k_2$. Then, we have $A_{k_1k_2} = A_{k_2k_1}^T = \sum_{p=1}^{P}\tilde{A}_p^{k_1k_2}$, where $\tilde{A}_p^{k_1k_2} = (\tilde{A}_p^{k_2k_1})^T = \left[\tilde{A}_p^{k_1k_2}(i,j)\right]_{P\times P} \in \mathbb{R}^{P\times P}$. When $k_2 < N$, for $i,j \in \{1,\dots,P\}\setminus p$ we have $\tilde{A}_p^{k_1k_2}(i,j) = 0.5\Gamma_p(k_1)$; $\tilde{A}_p^{k_1k_2}(p,j) = -0.5q_p^{\text{c}}/\kappa_p^{\text{jam}}$ for $j \in \{1,\dots,P\}\setminus p$; whereas $\tilde{A}_p^{k_1k_2}(i,p) = 0$ for all $i \in \{1,\dots,P\}$. To add, when $k_2 = N$, for $i \in \{1,\dots,P\}\setminus p$ and $j < p$, one gets $\tilde{A}_p^{k_1N}(i,j) = 0.5\Gamma_p(k_1)$; for $i = p$ and $j < p$, $\tilde{A}_p^{k_1N}(p,j) = -0.5q_p^{\text{c}}/\kappa_p^{\text{jam}}$; and for $j \geq p$ and every i, one gets $\tilde{A}_p^{k_1N}(i,j) = 0$.

In addition, $\mathbf{B_N} = [B_k]_{NP\times 1}$ with $B_k = \sum_{p=1}^{P}\chi_p\kappa_p^{\text{jam}}\tilde{B}_p^k$, $k \in \{1,\dots,N\}$, and $\tilde{B}_p^k = \left[\tilde{B}_p^k(i)\right]_{P\times 1}$. Note that $\tilde{B}_p^k(i)$ is the multiplier of $g_i(k)$ that appears in the delay of Phase p, D_p. When $k < N$, for $i \in \{1,\dots,P\}\setminus p$, we obtain $\tilde{B}_p^k(i) = \delta_{p,1}(1) + \sum_{m=1}^{k-1}\Gamma_p(m)L + (N-k)\,\Gamma_p(k)L + \Gamma_p(k)\sum_{j=1}^{p-1}l_i$; and $\tilde{B}_p^k(p) = -(N-k)q_p^{\text{c}}/\kappa_p^{\text{jam}}L$. Furthermore, for $k = N$ we get $\tilde{B}_p^N(i) = \delta_{p,1}(1) + \sum_{m=1}^{N-1}\Gamma_p(m)L + \Gamma_p(N)\sum_{j=1}^{p-1}l_j$ for $i < p$; $\tilde{B}_p^N(i) = \Gamma_p(N)\sum_{j=p}^{P}l_j$ for $i > p$, and $\tilde{B}_p^N(p) = 0$.

Finally, $\mathbf{C_N} = \sum_{k=1}^{N}\sum_{p=1}^{P}\chi_p\kappa_p^{\text{jam}}C_p^k$, where $C_p^k = \delta_{p,1}(1)L + \sum_{m=1}^{k-1}\Gamma_p(m)L^2 + 0.5\Gamma_p(k)L^2$ for $k < N$, and for $k = N$ we get $C_p^N = \left(\delta_{p,1}(1) + \sum_{m=1}^{N-1}\Gamma_p(m)L\right)\sum_{j=1}^{p-1}l_j + 0.5\Gamma_p(N)\left((\sum_{j=1}^{p-1}l_j)^2 + (\sum_{j=p}^{P}l_j)^2\right)$.

B. Parameters of the Modelled Constraints

Parameters of the linear constraints, demonstrated in (12), are arithmetically recognized in the following. It is assumed hereafter that $k' \in \{1,\dots,N\}$ and $j' \in \{1,\dots,P\}$. $H_{p,1}^k = \left[\tilde{H}_{k',p,1}^k\right]_{1\times NP} \in \mathbb{R}^{1\times NP}$, where $\tilde{H}_{k',p,1}^k = \left[\tilde{H}_{k',p,1}^k(j')\right]_{1\times P} \in \mathbb{R}^{1\times P}$, and for $k' < k$

$$\tilde{H}_{k',p,1}^k(j') = \begin{cases}\Gamma_p(k') & j' \neq p,\\ -q_p^{\text{c}}/\kappa_p^{\text{jam}} & j' = p,\end{cases}$$

for $k' = k$

$$\tilde{H}_{k',p,1}^k(j') = \begin{cases}\Gamma_p(k') & j' < p,\\ -q_p^{\text{c}}/\kappa_p^{\text{jam}} & j' = p,\\ 0 & j' > p,\end{cases}$$

and for $k' > k$, $\tilde{H}_{k',p,1}^k(j') = 0$. Moreover,

$$b_{p,1}^k = -\delta_{p,1}(1) - \sum_{m=1}^{k-1}\Gamma_p(m)L - \Gamma_p(k)\sum_{j=1}^{p-1}l_j.$$

$H^k_{p,2} = \left[\tilde{H}^k_{k',p,2}\right]_{1\times NP}$, where $\tilde{H}^k_{k',p,2} = \left[\tilde{H}^k_{k',p,2}(j')\right]_{1\times P}$, and for $k' < k$

$$\tilde{H}^k_{k',p,2}(j') = \begin{cases} \sum_{r=1}^{P} \Gamma_r(k') & j' \neq p, \\ -\sum_{r=1}^{P} q^{\mathrm{c}}_r/\kappa^{\mathrm{jam}}_r & j' = p, \end{cases}$$

for $k' = k$

$$\tilde{H}^k_{k',p,2}(j') = \begin{cases} \sum_{r=1}^{P} \Gamma_r(k') & j' < p, \\ -\sum_{r=1}^{P} q^{\mathrm{c}}_r/\kappa^{\mathrm{jam}}_r & j' = p, \\ 0 & j' > p, \end{cases}$$

and for $k' > k$, $\tilde{H}^k_{k',p,2}(j') = 0$. Moreover,

$$b^k_{p,2} = -P\delta_{p,1}(1) - \sum_{r=1}^{P}\sum_{m=1}^{k-1} \Gamma_r(m)L - \sum_{r=1}^{P} \Gamma_r(k) \sum_{j=1}^{p-1} l_j.$$

$H^k_{p,3} = \left[\tilde{H}^k_{k',p,3}\right]_{1\times NP}$, where $\tilde{H}^k_{k',p,3} = \left[\tilde{H}^k_{k',p,3}(j')\right]_{1\times P}$, and for $k' \neq \{k, k+1\}$, $\tilde{H}^k_{k',p,3}(j') = \mathbf{0}$,

$$\tilde{H}^k_{k,p,3}(j') = \begin{cases} 0 & j' \leq p, \\ -\Gamma_p(k) & j' > p, \end{cases}$$

and

$$\tilde{H}^k_{k+1,p,3}(j') = \begin{cases} -\Gamma_p(k+1) & j' < p, \\ q^{\mathrm{c}}_p/\kappa^{\mathrm{jam}}_p & j' = p, \\ 0 & j' > p. \end{cases}$$

Moreover,

$$b^k_{p,3} = \Gamma_p(k) \sum_{j=p}^{P} l_j + \Gamma_p(k+1) \sum_{j=1}^{p-1} l_j.$$

The undersaturation constraint parameters in (14) are defined as follows: $H^k_{p,5} = \left[\tilde{H}^k_{k',p,5}\right]_{1\times NP}$, where $\tilde{H}^k_{k',p,5} = \left[\tilde{H}^k_{k',p,5}(j')\right]_{1\times P}$, $\tilde{H}^k_{k',p,5}(j') = 0$ for $k' \neq k$, and for $k' = k$,

$$\tilde{H}^k_{k',p,5}(j') = \begin{cases} 1 - \eta_p(k) - 1/(P-1) & j' \neq p, \\ 1 & j' = p. \end{cases}$$

Furthermore, $b^k_{p,5} = -(1 - \eta_p(k) - 1/(P-1))L - \frac{2-P}{P-1} l_p$.

Eventually, the spillback avoidance constraints (15a) and (15b) are elaborated in the sequel. $H^k_{p,6} = \left[\tilde{H}^k_{k',p,6}\right]_{1\times NP}$, $\tilde{H}^k_{k',p,6} = \left[\tilde{H}^k_{k',p,6}(j')\right]_{1\times P}$; for all $k' < k$:

$$\tilde{H}^k_{k',p,6}(j') = \begin{cases} -\Gamma_p(k') & j' \neq p, \\ q^{\mathrm{c}}_p/\kappa^{\mathrm{jam}}_p & j' = p, \end{cases}$$

for $k' = k$:

$$\tilde{H}^k_{k',p,6}(j') = \begin{cases} -\Gamma_p(k') & j' < p, \\ 0 & j' \geq p, \end{cases}$$

and $\tilde{H}^k_{k',p,6}(j') = 0$ for $k' > k$. We also have $b^k_{p,6} = -\beta_p\Delta_p + \delta_{p,1}(1) + \sum_{m=1}^{k-1} \Gamma_p(m)L + \Gamma_p(N)\sum_{j=1}^{p-1} l_j$. $H^k_{p,7} = \left[\tilde{H}^k_{k',p,7}\right]_{1\times NP}$, $\tilde{H}^k_{k',p,7} = \left[\tilde{H}^k_{k',p,7}(j')\right]_{1\times P}$; for $k' \leq k$:

$$\tilde{H}^k_{k',p,7}(j') = \begin{cases} -\Gamma_p(k') & j' \neq p, \\ q^{\mathrm{c}}_p/\kappa^{\mathrm{jam}}_p & j' = p, \end{cases}$$

and $\tilde{H}^k_{k',p,7}(j') = 0$ for $k' > k$. To add, $b^k_{p,7} = -\beta_p\Delta_p + \delta_{p,1}(1) + \sum_{m=1}^{k} \Gamma_p(m)L$.

ACKNOWLEDGMENT

The authors thank Dr. Sajjad Shafiei for helping with the microsimulation experiments.

REFERENCES

[1] J. Haddad, P.-O. Gutman, I. Ioslovich, and D. Mahalel, "Discrete dynamic optimization of N-stages control for isolated signalized intersections," *Control Eng. Pract.*, vol. 21, no. 11, pp. 1553–1563, Nov. 2013.

[2] R. Mohajerpoor, M. Saberi, and M. Ramezani, "Delay variability optimization using shockwave theory at an undersaturated intersection," *IFAC-PapersOnLine*, vol. 50, no. 1, pp. 5289–5294, Jul. 2017.

[3] C. F. Daganzo, L. J. Lehe, and J. Argote-Cabanero, "Adaptive offsets for signalized streets," *Transp. Res. B, Methodol.*, vol. 117, pp. 926–934, Nov. 2018.

[4] J. Haddad and D. Mahalel, "Offset effects on the capacity of paired signalised intersections during oversaturated conditions," *Transportmetrica A, Transp. Sci.*, vol. 10, no. 8, pp. 740–758, Sep. 2014.

[5] M. Saeedmanesh and N. Geroliminis, "Dynamic clustering and propagation of congestion in heterogeneously congested urban traffic networks," *Transp. Res. Proc.*, vol. 23, pp. 962–979, Jan. 2017.

[6] R. Mohajerpoor, M. Saberi, H. L. Vu, T. M. Garoni, and M. Ramezani, "H_∞ robust perimeter flow control in urban networks with partial information feedback," *Transp. Res. B, Methodol.*, vol. 137, pp. 47–73, Jul. 2020.

[7] S. Lee, S. C. Wong, and P. Varaiya, "Group-based hierarchical adaptive traffic-signal control. Part I: Formulation," *Transp. Res. B, Methodol.*, vol. 105, pp. 1–18, Nov. 2017.

[8] M. Rinaldi, "Controllability of transportation networks," *Transp. Res. B, Methodol.*, vol. 118, pp. 381–406, Dec. 2018.

[9] S. Shepherd, "A review of traffic signal control," Inst. Transp. Stud., Univ. Leeds, Leeds, U.K., Tech. Rep. 349, Jan. 1992.

[10] K. Wood, "Urban traffic control: Systems review," Berkshire, Crowthorne, U.K., Tech. Rep. 41, 1993.

[11] S. Chen, H. Xu, and H. Liu, "Timing oversaturated signals: What can we learn from classic and state-of-the-art signal control models," *J. Transp. Syst. Eng. Inf. Technol.*, vol. 13, no. 1, pp. 97–110, Feb. 2013.

[12] N. Geroliminis, J. Haddad, and M. Ramezani, "Optimal perimeter control for two urban regions with macroscopic fundamental diagrams: A model predictive approach," *IEEE Trans. Intell. Transp. Syst.*, vol. 14, no. 1, pp. 348–359, Mar. 2013.

[13] Y. Li, R. Mohajerpoor, and M. Ramezani, "Perimeter control with real-time location-varying cordon," *Transp. Res. B, Methodol.*, vol. 150, pp. 101–120, Aug. 2021.

[14] J. Haddad, "Optimal perimeter control synthesis for two urban regions with aggregate boundary queue dynamics," *Transp. Res. B, Methodol.*, vol. 96, pp. 1–25, Feb. 2017.

[15] R. Akcelik, "Traffic signals: Capacity and timing analysis," Austral. Road Res. Board, Vermont South, VIC, Australia, Tech. Rep. ARR 123, 1981.

[16] R. Mohajerpoor, M. Saberi, and M. Ramezani, "Analytical derivation of the optimal traffic signal timing: Minimizing delay variability and spillback probability for undersaturated intersections," *Transp. Res. B, Methodol.*, vol. 119, pp. 45–68, Jan. 2019.

[17] H. David and A. John, *Synchro Studio 7: Traffic Signal Software—User Guide*. Albany, CA, USA: Trafficware, 2006.

[18] N. H. Gartner, *OPAC: A Demand-Responsive Strategy for Traffic Signal Control*. Washington, DC, USA: Transportation Research Record, 1983.

[19] D. Hale, *Traffic Network Study Tool TRANSYT-7F*. Gainesville, FL, USA: Center in the Univ. of Florida, 2005.

[20] P. Hunt, D. Robertson, R. Bretherton, and M. C. Royle, "The scoot on-line traffic signal optimisation technique," *Traffic Eng. Control*, vol. 23, no. 4, pp. 190–192, 1982.

[21] P. Lowrie, "Scats, Sydney co-ordinated adaptive traffic system: A traffic responsive method of controlling urban traffic," Roads and Traffic Authority, Sydney, NSW, Australia, Tech. Rep., 1990.

[22] C. Cai, C. K. Wong, and B. G. Heydecker, "Adaptive traffic signal control using approximate dynamic programming," *Transp. Res. C, Emerg. Technol.*, vol. 17, no. 5, pp. 456–474, Oct. 2009.

[23] L. Zhang, Y. Yin, and Y. Lou, "Robust signal timing for arterials under day-to-day demand variations," *Transp. Res. Rec., J. Transp. Res. Board*, vol. 2192, no. 1, pp. 156–166, Dec. 2010.

[24] R. Mohebifard and A. Hajbabaie, "Optimal network-level traffic signal control: A benders decomposition-based solution algorithm," *Transp. Res. B, Methodol.*, vol. 121, pp. 252–274, Mar. 2019.

[25] M. Noaeen, R. Mohajerpoor, B. H. Far, and M. Ramezani, "Real-time decentralized traffic signal control for congested urban networks considering queue spillbacks," *Transp. Res. C, Emerg. Technol.*, vol. 133, Dec. 2021, Art. no. 103407.

[26] T. Wongpiromsarn, T. Uthaicharoenpong, Y. Wang, E. Frazzoli, and D. Wang, "Distributed traffic signal control for maximum network throughput," in *Proc. 15th Int. IEEE Conf. Intell. Transp. Syst.*, Sep. 2012, pp. 588–595.

[27] P. Varaiya, "Max pressure control of a network of signalized intersections," *Transp. Res. C, Emerg. Technol.*, vol. 36, pp. 177–195, Nov. 2013.

[28] J. Gregoire, X. Qian, E. Frazzoli, A. D. L. Fortelle, and T. Wongpiromsarn, "Capacity-aware backpressure traffic signal control," *IEEE Trans. Control Netw. Syst.*, vol. 2, no. 2, pp. 164–173, Jun. 2015.

[29] L. Li and S. E. Jabari, "Position weighted backpressure intersection control for urban networks," *Transp. Res. B, Methodol.*, vol. 128, pp. 435–461, Oct. 2019.

[30] A. Kouvelas, J. Lioris, S. Fayazi, and P. Varaiya, "Maximum pressure controller for stabilizing queues in signalized arterial networks," *Transp. Res. Rec. J. Transp. Res. Board*, vol. 2421, no. 1, pp. 133–141, 2014.

[31] D. C. Gazis, "Optimum control of a system of oversaturated intersections," *Oper. Res.*, vol. 12, no. 6, pp. 815–831, 1964.

[32] P. G. Michalopoulos and G. Stephanopoulos, "Oversaturated signal systems with queue length constraints—I: Single intersection," *Transp. Res.*, vol. 11, no. 6, pp. 413–421, Dec. 1977.

[33] T.-H. Chang and G.-Y. Sun, "Modeling and optimization of an oversaturated signalized network," *Transp. Res. B, Methodol.*, vol. 38, no. 8, pp. 687–707, Sep. 2004.

[34] K. Aboudolas, M. Papageorgiou, A. Kouvelas, and E. Kosmatopoulos, "A rolling-horizon quadratic-programming approach to the signal control problem in large-scale congested urban road networks," *Transp. Res. C, Emerg. Technol.*, vol. 18, no. 5, pp. 680–694, Oct. 2010.

[35] C. Diakaki, M. Papageorgiou, and K. Aboudolas, "A multivariable regulator approach to traffic-responsive network-wide signal control," *Control Eng. Pract.*, vol. 10, no. 2, pp. 183–195, Feb. 2002.

[36] M. Papageorgiou, C. Diakaki, V. Dinopoulou, A. Kotsialos, and Y. Wang, "Review of road traffic control strategies," *Proc. IEEE*, vol. 91, no. 12, pp. 2043–2067, Dec. 2003.

[37] T. Tettamanti, T. Luspay, B. Kulcsár, T. Péni, and I. Varga, "Robust control for urban road traffic networks," *IEEE Trans. Intell. Transp. Syst.*, vol. 15, no. 1, pp. 385–398, Feb. 2014.

[38] W. Xiang, J. Xiao, and Y. Jiang, "Real-time signalization for an oversaturated intersection via static state feedback control: A switched system approach," *J. Franklin Inst.*, vol. 352, no. 8, pp. 3304–3324, Aug. 2015.

[39] H. K. Lo, "A novel traffic signal control formulation," *Transp. Res. A, Policy Pract.*, vol. 33, no. 6, pp. 433–448, 1999.

[40] M. J. Lighthill and G. B. Whitham, "On kinematic waves. II. A theory of traffic flow on long crowded roads," *Proc. Roy. Soc. London A, Math. Phys. Sci.*, vol. 229, no. 1178, pp. 317–345, 1955.

[41] F. V. Webster, "Traffic signal settings," Her Majesty's Stationery Office, Dept. Sci. Ind. Res., Road Res. Lab., Tech. Rep. 39, 1958.

[42] M. Saberi *et al.*, "A simple contagion process describes spreading of traffic jams in urban networks," *Nature Commun.*, vol. 11, no. 1, p. 1616, Dec. 2020.

[43] M. Ramezani, N. de Lamberterie, A. Skabardonis, and N. Geroliminis, "A link partitioning approach for real-time control of queue spillbacks on congested arterials," *Transportmetrica B, Transp. Dyn.*, vol. 5, no. 2, pp. 177–190, 2016.

[44] W. Ma, K. An, and H. K. Lo, "Multi-stage stochastic program to optimize signal timings under coordinated adaptive control," *Transp. Res. C, Emerg. Technol.*, vol. 72, pp. 342–359, Nov. 2016.

[45] A. Ermagun and D. Levinson, "Spatiotemporal traffic forecasting: Review and proposed directions," *Transp. Rev.*, vol. 38, no. 6, pp. 786–814, Nov. 2018.

[46] H. Nguyen, C. Bentley, L. M. Kieu, Y. Fu, and C. Cai, "Deep learning system for travel speed predictions on multiple arterial road segments," *Transp. Res. Rec., J. Transp. Res. Board*, vol. 2673, no. 4, pp. 145–157, Apr. 2019.

[47] P. G. Michalopoulos, G. Stephanopoulos, and G. Stephanopoulos, "An application of shock wave theory to traffic signal control," *Transp. Res. B, Methodol.*, vol. 15, no. 1, pp. 35–51, Feb. 1981.

[48] M. Ramezani and N. Geroliminis, "Queue profile estimation in congested urban networks with probe data," *Comput.-Aided Civil Infrastruct. Eng.*, vol. 30, no. 6, pp. 414–432, 2015.

[49] R. Mohajerpoor and M. Ramezani, "Mixed flow of autonomous and human-driven vehicles: Analytical headway modeling and optimal lane management," *Transp. Res. C, Emerg. Technol.*, vol. 109, pp. 194–210, Dec. 2019.

[50] J. Chen and S. Burer, "Globally solving nonconvex quadratic programming problems via completely positive programming," *Math. Program. Comput.*, vol. 4, no. 1, pp. 33–52, Mar. 2012.

[51] W. Xia, J. C. Vera, and L. F. Zuluaga, "Globally solving nonconvex quadratic programs via linear integer programming techniques," *INFORMS J. Comput.*, vol. 32, no. 1, pp. 40–56, Jan. 2020.

[52] P. Belotti, J. Lee, L. Liberti, F. Margot, and A. Wächter, "Branching and bounds tightening techniques for non-convex MINLP," *Optim. Methods Softw.*, vol. 24, nos. 4–5, pp. 597–634, 2009.

[53] M. Fampa, J. Lee, and W. Melo, "On global optimization with indefinite quadratics," *EURO J. Comput. Optim.*, vol. 5, no. 3, pp. 309–337, 2017.

Reza Mohajerpoor received the B.Sc. degree in mechanical engineering, in 2008, the M.Sc. degree in mechatronics engineering, in 2011, and the Ph.D. degree in control science, in 2016. He completed postdoctoral studies on ITS topics at Monash University and The University of Sydney, in 2019. He was a Research Scientist with Data61, CSIRO, from 2019 to 2021, working on ITS and applications of machine learning on transport systems. He is currently a Principal Data Scientist with the Insurance Australia Group (IAG). His research interests include dynamic modeling and control of urban traffic networks, autonomous vehicles, and applied machine learning.

Chen Cai is currently the Leader of the Transport Analytics Group, Data61 (CSIRO), and the Leader of the Data61's Business Initiatives with Transport and Logistics. Being a pioneer in adopting AI for transport, he co-founded group, in 2013, and led it to grow into one of Australia's leading research units. He is a Board Director of Intelligent Transport Systems Australia, the peak-body of the nation's ITS industry. He has led his group to earn more than $10 million external revenue to Data61, since 2016, including the Award of the NSW Premier's Innovation Initiative.

Mohsen Ramezani received the B.Sc. and M.Sc. degrees in electrical engineering and control systems from the University of Tehran, Iran, in 2008 and 2010, respectively, and the Ph.D. degree in transportation from the École Polytechnique Fédérale de Lausanne, Switzerland, in 2014. He is currently a Senior Lecturer with the Transport Laboratory, School of Civil Engineering, The University of Sydney. His research interests include point to point transport services, traffic control, data analytics, and traffic flow theory and operations. He is an Australian Research Council (ARC) Discovery Early Career Research Award (DECRA) Fellow. He was a recipient of the 2015 IEEE Intelligent Transportation Systems Society 1st Prize Best Ph.D. Dissertation.